

## Article

# Effects of Phosphorus Addition on the Hydrophobicity and Catalytic Performance in Methane Combustion of $\theta$ -Al<sub>2</sub>O<sub>3</sub> Supported Pd Catalysts

Wei Xiong<sup>1</sup>, Jun Wang<sup>1</sup>, Yunhao Wang<sup>1</sup>, Jianqiang Wang<sup>1</sup>, Chen Wang<sup>2</sup> , Gurong Shen<sup>3,\*</sup>   
and Meiqing Shen<sup>1,4,\*</sup>

<sup>1</sup> Key Laboratory for Green Chemical Technology of the State Education Ministry, School of Chemical Engineering and Technology, Tianjin University, Tianjin 300354, China

<sup>2</sup> School of Environmental and Safety Engineering, North University of China, Taiyuan 030051, China

<sup>3</sup> School of Materials Science and Engineering, Tianjin University, Tianjin 257400, China

<sup>4</sup> National Rare Earth Catalysis Research Institute, Dongying 257000, China

\* Correspondence: gr\_shen@tju.edu.cn (G.S.); mqshen@tju.edu.cn (M.S.)

**Abstract:** A series of xP $\theta$ -Al<sub>2</sub>O<sub>3</sub> supports modified with different amounts of phosphorus element were prepared and taken as supports of palladium catalysts for methane catalytic combustion. The impacts of phosphorus additives on the hydrophobicity of Pd/xP $\theta$ -Al<sub>2</sub>O<sub>3</sub> and its performance of methane catalytic combustion in the absence of and presence of 8% water were systematically studied. It was found that the hydrophobicity of xP $\theta$ -Al<sub>2</sub>O<sub>3</sub> changed with the increase of phosphorus content, which had a significant effect on the activity of methane catalytic combustion. The incorporation of phosphorus replaced the hydroxyl groups on the surface of Al<sub>2</sub>O<sub>3</sub> in the form of phosphates, thus changing the density of hydroxyl groups of Al<sub>2</sub>O<sub>3</sub> support. TGA, NH<sub>3</sub>-TPD, IR, and XPS were employed to illustrate the process of phosphate replacement. xP $\theta$ -Al<sub>2</sub>O<sub>3</sub> with less than 1 wt.% phosphorus content had better hydrophobicity than the unmodified  $\theta$ -Al<sub>2</sub>O<sub>3</sub> and Pd/xP $\theta$ -Al<sub>2</sub>O<sub>3</sub>, therefore had better performance for methane catalytic combustion, which was attributed to the substitution of hydroxyl groups on the surface of  $\theta$ -Al<sub>2</sub>O<sub>3</sub> by PO<sub>4</sub><sup>3-</sup> and HPO<sub>4</sub><sup>2-</sup>. However, when the phosphorus content of Al<sub>2</sub>O<sub>3</sub> was higher than 1 wt.%, the substitution of H<sub>2</sub>PO<sub>4</sub><sup>-</sup> began to dominate, which would lead to poorer hydrophobicity and catalytic performance. This work will guide the design of methane catalytic combustion catalysts resistant to water inhibition problem.

**Keywords:** phosphorus additive; methane catalytic combustion; water inhibition; palladium-based catalyst; hydrophobicity



check for updates

**Citation:** Xiong, W.; Wang, J.; Wang, Y.; Wang, J.; Wang, C.; Shen, G.; Shen, M. Effects of Phosphorus Addition on the Hydrophobicity and Catalytic Performance in Methane Combustion of  $\theta$ -Al<sub>2</sub>O<sub>3</sub> Supported Pd Catalysts. *Catalysts* **2023**, *13*, 709. <https://doi.org/10.3390/catal13040709>

Academic Editor: Leonarda Liotta

Received: 28 February 2023

Revised: 21 March 2023

Accepted: 5 April 2023

Published: 7 April 2023



**Copyright:** © 2023 by the authors. Licensee MDPI, Basel, Switzerland. This article is an open access article distributed under the terms and conditions of the Creative Commons Attribution (CC BY) license (<https://creativecommons.org/licenses/by/4.0/>).

## 1. Introduction

In recent years, lean-burn natural gas vehicles (NGVs) have attracted extensive attention due to their high fuel-efficiency and low pollution [1,2], however, lean-burn operation of a natural gas engine results in incomplete combustion of methane [3,4]. Methane has over 20 times larger global warming potential than carbon dioxide [5,6], which makes the control of methane emissions compulsory. Removal of unburned methane by catalytic oxidation has been proved the most effective method to address the problems [7]. Among the various catalysts for methane catalytic combustion, palladium-based catalysts have been widely used due to their high methane catalytic combustion conversion at low temperatures and Pd/Al<sub>2</sub>O<sub>3</sub> catalysts are considered to be the most efficient catalysts for methane oxidation. Methane combustion catalysts must achieve an ignition temperature of 200–300 °C and complete oxidation temperature of 500–550 °C; however, natural gas vehicle exhaust contains a lot of water vapor, resulting in the activity of the catalyst being severely inhibited at low temperatures (<450 °C) [8,9]. Studies have shown that the accumulation of hydroxyl groups is the main cause of water inhibition problems [10,11], thus improving the

hydrophobicity of the carrier or employing hydrophobic zeolite is the key factor in solving the water inhibition problem of methane catalytic combustion catalysts [12,13].

So far, many strategies have been developed to solve the water inhibition problem. One effective strategy is regulating the surface properties of the supports by adding additives [14]. Olsson et al. [15] showed that the addition of Ba could inhibit the formation of hydroxyl on the surface of  $\text{Al}_2\text{O}_3$ , thus improving the activity of the catalyst. The addition of Ni can form a  $\text{NiAl}_2\text{O}_4$  structure [16,17], improving the dispersion of PdO and inhibiting the accumulation of  $\text{OH}^-$  species on the surface of PdO particles during the reaction. Metallic element additives have been studied a lot, but non-metallic elements are rarely studied, such as phosphorus element, which has been proven to stabilize the structure of  $\text{Al}_2\text{O}_3$  and inhibit the phase transition of  $\gamma\text{-Al}_2\text{O}_3$  to  $\alpha\text{-Al}_2\text{O}_3$  under high temperatures [18]. The incorporation of phosphorus will decorate the hydroxyl group on the alumina surface and introduce the P-OH groups [19], which will change the distribution of Lewis acid and Brønsted acid sites on the  $\text{Al}_2\text{O}_3$  surface. However, there are few studies focusing on the effect of the content of phosphorus on the supports, especially in the low-phosphorus content range.

Methane catalytic combustion catalyst Pd/ $\gamma\text{-Al}_2\text{O}_3$  has been widely studied, but  $\theta\text{-Al}_2\text{O}_3$  used as a carrier for methane oxidation is rarely studied. Atsushi et al. [20] studied the influence of the phases of  $\text{Al}_2\text{O}_3$  on methane combustion in the presence of water, and found that  $\theta\text{-Al}_2\text{O}_3$  and  $\alpha\text{-Al}_2\text{O}_3$  had better methane oxidation activity due to their higher hydrophobicity. However, the specific surface area of  $\alpha\text{-Al}_2\text{O}_3$  is too small, which is not conducive to the dispersion of precious metal Pd, which is one of the important factors affecting the performance of the catalyst. Therefore,  $\theta\text{-Al}_2\text{O}_3$  is more suitable as a carrier for methane oxidation because it has better hydrophobic properties than  $\gamma\text{-Al}_2\text{O}_3$  and larger specific surface area than  $\alpha\text{-Al}_2\text{O}_3$ .

In this work, different amounts of phosphorus element were doped on  $\theta\text{-Al}_2\text{O}_3$  support by incipient wetness impregnation method. TGA,  $\text{NH}_3\text{-TPD}$ , FT-IR and XPS were employed to study the effect of phosphorus on  $\theta\text{-Al}_2\text{O}_3$  supports. On this basis, the Pd-based catalysts were prepared using P-modified  $\theta\text{-Al}_2\text{O}_3$  as the support. The methane catalytic combustion activity of the catalysts in the absence and presence of 8% water and the effect of phosphorus on the hydrophobicity of the catalysts were studied. This study could be instructive for the development of high-performance methane catalytic combustion catalysts under wet conditions.

## 2. Results and Discussion

### 2.1. Characterization of the Supports

The phosphorus element contents of the supports were determined by ICP-OES and the results are shown in Table S1.

Powder X-ray diffraction (XRD) patterns of the  $\text{Al}_2\text{O}_3$ , which was calcined at different temperatures, is displayed in Figure S1. With the increase of calcination temperature,  $\gamma\text{-Al}_2\text{O}_3$  began to transition to  $\theta$  phase and  $\alpha$  phase and the  $\gamma$  phase completely changed into  $\theta$  phase at 1050 °C. XRD patterns of xP $\theta\text{-Al}_2\text{O}_3$  are displayed in Figure S2. With the increase of P content, no new crystal structure appeared, implying that the doping method and impregnation method is a surface modification strategy.

The textural properties of xP $\theta\text{-Al}_2\text{O}_3$  are given in Table S2. With the increase of P element, the specific surface area and pore volume of the carrier decreased gradually. This phenomenon was more obvious when the P content was above 1 wt.%, The possible reason is that excessive P will block some of the pores of  $\text{Al}_2\text{O}_3$ , resulting in the decrease of pore volume [18].

In order to explore the influence of phosphorus addition on the hydrophilicity of  $\text{Al}_2\text{O}_3$ , TGA test was conducted and results are shown in Figure 1. In fact, the  $\text{H}_2\text{O-TPD}$  test would usually be used to illustrate the hydrophobicity of the sample. Since we could not perform the  $\text{H}_2\text{O-TPD}$  test, we chose to employ the TGA test. These two methods are essentially the same. Both of them first need to let the sample adsorb water at a low temperature

until saturation, and then carry out temperature-programmed desorption. Briefly, prior to the TGA test, the supports were treated with constant temperature at 80 °C and 70% humidity until water adsorption saturation. Therefore, the hydrophobic characteristics of the supports could be reflected by the desorption amount of water measured by TGA. As shown in Figure 1 and Table S3, the weight loss curves of the supports between 80 °C and 300 °C was tested, which reflects the desorption of physically and chemically adsorbed water [21]. The support with 0.1 wt.% P content had the least amount of water desorption and therefore had the best hydrophobicity. With the increase of P content, the supports became more hydrophilic. However, for the unmodified  $\theta$ -Al<sub>2</sub>O<sub>3</sub>, the amount of desorption water was larger than that of the support with 0.6 wt.% phosphorus content, and smaller than that of the support with 1 wt.% P content, indicating that the hydrophobicity of the  $\theta$ -Al<sub>2</sub>O<sub>3</sub> was improved when less P (<1 wt.%) modified the supports.

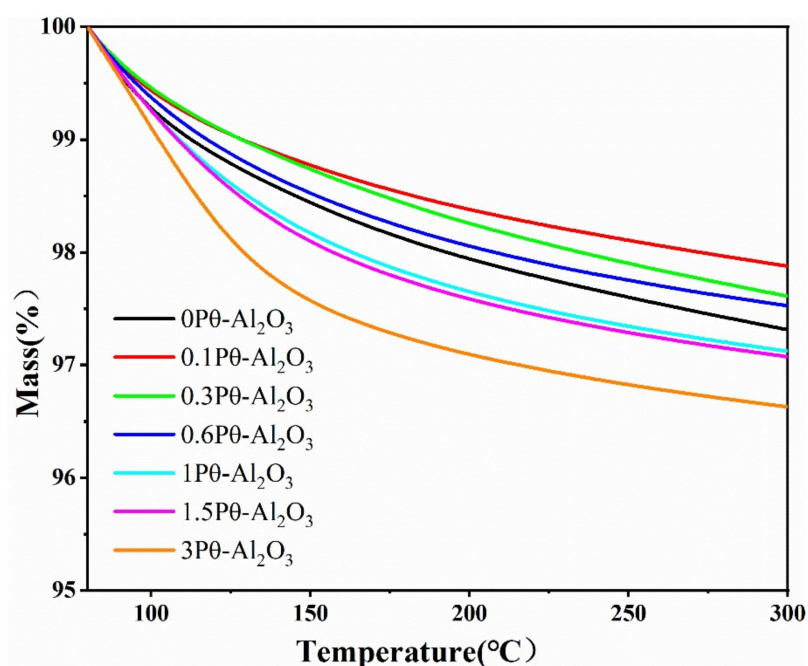
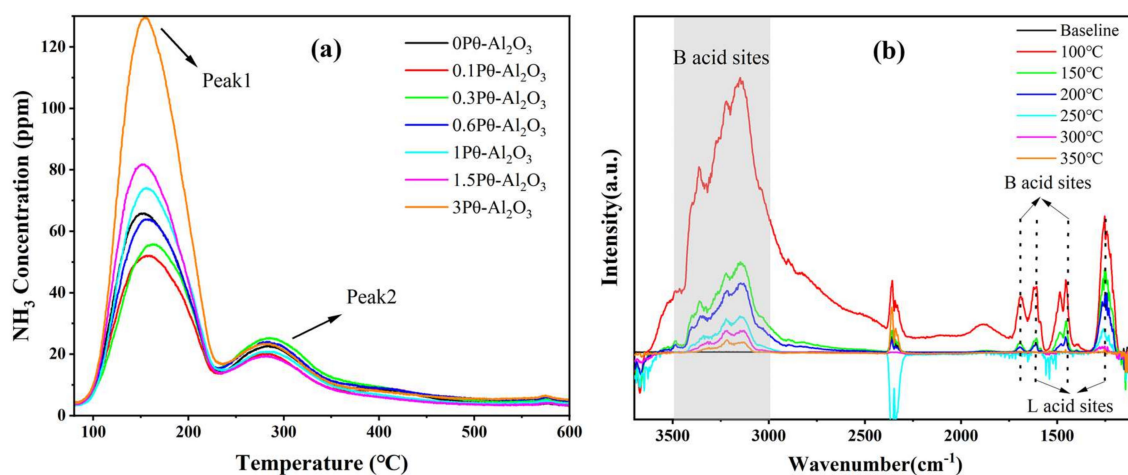


Figure 1. The weight loss curves of supports measured by TGA.

There are a lot of surface hydroxyl groups on the surface of alumina, which directly determines its hydrophobic properties. Therefore, in order to illustrate the effect of P modification on the hydrophobic performance of  $\theta$ -Al<sub>2</sub>O<sub>3</sub>, it is necessary to further explore the change of hydroxyl density on the surface of  $\theta$ -Al<sub>2</sub>O<sub>3</sub> with the increase of P content. The content of hydroxyl groups on the surface of alumina is difficult to accurately quantify by experimental methods. Here, the changes of hydroxyl groups on the surface of supports were illustrated by NH<sub>3</sub>-TPD test. As shown in Figure 2a, the desorption curves of NH<sub>3</sub> had two peaks. The peak maximum of the first peak is within the range of 150–160 °C, so peak 1 is classified as weak acid [22]. The peak maximum of the second peak is about 280 °C, which is classified as medium strength acid [23]. In order to further assign the desorption peak of NH<sub>3</sub>, NH<sub>3</sub>-IR test was conducted.  $\theta$ -Al<sub>2</sub>O<sub>3</sub> adsorbed NH<sub>3</sub> at 100 °C to reach saturation and the infrared absorption signal of NH<sub>3</sub> reached the strongest at this time. Then, N<sub>2</sub> was purged for 30 min until stable, in which case the infrared absorption signal of NH<sub>3</sub> gradually weakened. It can be considered that the physically adsorbed NH<sub>3</sub> had been completely desorbed after  $\theta$ -Al<sub>2</sub>O<sub>3</sub> was purged by N<sub>2</sub>. As shown in Figure 2b, the desorption spectra of NH<sub>3</sub> were collected at different temperatures and the NH<sub>3</sub> desorbed in this process was mainly chemisorbed NH<sub>3</sub>. When the temperature began to rise from 100 °C to 150 °C, the infrared adsorption peak of NH<sub>3</sub> was significantly weakened, which indicated that the NH<sub>3</sub> on the support had undergone chemical desorption.



**Figure 2.** (a)  $\text{NH}_3$ –TPD profiles of the supports. (b)  $\text{NH}_3$ –IR profiles of  $\theta\text{-Al}_2\text{O}_3$ .

The infrared absorption peaks in the range of  $3000\text{--}3500\text{ cm}^{-1}$  mainly correspond to the Brønsted acids produced by the hydroxyl groups on the surface of  $\text{Al}_2\text{O}_3$  [24], which correspond to the first peak in the  $\text{NH}_3$ -TPD curve. Therefore, the change of hydroxyl groups on the surface of  $\text{Al}_2\text{O}_3$  can be explained by the change of the desorption amount of  $\text{NH}_3$  at the first peak tested by  $\text{NH}_3$ -TPD. The quantitative results of peak 1 are shown in Table S4. It is worth noting that we did not know the proportion of  $\text{NH}_3$  molecules adsorbed on the hydroxyl group, which meant that the content of hydroxyl groups on the surface of  $\text{Al}_2\text{O}_3$  could not be calculated simply by the desorption amount of  $\text{NH}_3$ . Therefore, the concept of relative surface hydroxyl density was introduced, which meant that the hydroxyl density on the surface of  $\theta\text{-Al}_2\text{O}_3$  was set to 1, and the relative value of other samples with respect to  $\theta\text{-Al}_2\text{O}_3$  was defined as the relative surface hydroxyl density of the carrier. According to the relative surface hydroxyl density, we can judge the hydrophobicity of the carrier. The support with 0.1 wt.% content of P element desorbed the lowest amount of  $\text{NH}_3$  and its relative surface hydroxyl density was the smallest, indicating that had the least surface hydroxyl content and it had the best hydrophobicity. On the other hand, the relationship between the content of P in the supports and the desorption amount of  $\text{NH}_3$  in the supports was consistent with the relationship of hydrophobicity reflected in the TG test, which indicated that the addition of a small amount of P (<1 wt.%) reduced the hydroxyl groups on the surface of  $\text{Al}_2\text{O}_3$ , and thus improved the hydrophobicity of  $\text{Al}_2\text{O}_3$ .

Based on the above results, the modification effect of P element on the  $\text{Al}_2\text{O}_3$  surface hydroxyl groups was explored. Figure S3 is the infrared spectrum of the carrier in the range of  $4000\text{ cm}^{-1}\text{--}700\text{ cm}^{-1}$ . The stretching vibration peaks of the hydroxyl groups are in the range of  $3670\text{ cm}^{-1}\text{--}3230\text{ cm}^{-1}$  [25], however, the peak in this range is a relatively wide peak, which cannot further distinguish the different types of hydroxyl groups. As shown in Figure 3 and the amplification of Figure S4 in the range of  $1600\text{ cm}^{-1}\text{--}700\text{ cm}^{-1}$ , the peaks attributed to P-OH in the range of  $847\text{ cm}^{-1}\text{--}1050\text{ cm}^{-1}$  cannot be distinguished due to the overlap with the peaks of Al-O. A new peak appeared in the range of  $1000\text{ cm}^{-1}\text{--}1174\text{ cm}^{-1}$  [26], which was attributed to the phosphorus–oxygen bond peak. It can be seen that with the increase of P content, the peak gradually became stronger and shifted toward the high wave number. Dong et al. [27] showed that the P element introduced by the impregnation method was mainly adsorbed on the surface of  $\text{Al}_2\text{O}_3$  in the form of phosphate, thus modifying the surface of  $\text{Al}_2\text{O}_3$ . Phosphate compounds have three basic forms:  $\text{PO}_4^{3-}$ ,  $\text{HPO}_4^{2-}$  and  $\text{H}_2\text{PO}_4^-$ . For phosphate compounds with different forms, the corresponding infrared wave number of phosphates was  $\text{PO}_4^{3-} < \text{HPO}_4^{2-} < \text{H}_2\text{PO}_4^-$  [25,28], which indicated that with the increase of P content,  $\text{PO}_4^{3-}$ ,  $\text{HPO}_4^{2-}$ ,  $\text{H}_2\text{PO}_4^-$  gradually appeared and dominated.

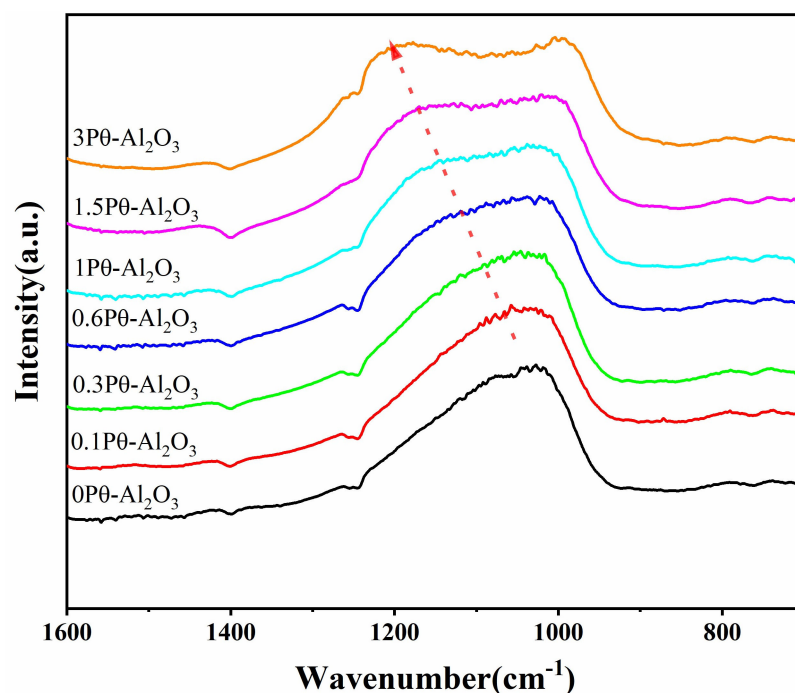


Figure 3. FT–IR profiles of supports.

The surface chemical states of the supports were investigated by XPS analysis. Figure 4 depicts the P 2p XPS spectra of the supports. Supports with 0 wt.% and 0.1 wt.% phosphorus content could not detect the presence of P element because there was no phosphorus element or too little phosphorus on the surface of the supports, which was lower than the detection limit of the XPS instrument. The P 2p signal appeared in the samples where the P element content was more than 0.3 wt.%, and the higher the content of phosphorus, the stronger the signal. This is because the P element in xPθ-Al<sub>2</sub>O<sub>3</sub> carrier was loaded by the impregnation method. After the carrier is calcined, phosphorus mainly existed on the surface of Al<sub>2</sub>O<sub>3</sub> in the form of phosphate compounds. Therefore, the higher the content of phosphorus on the surface of the support, the stronger the signal was detected. However, the P 2p spectrum of supports were not symmetric peaks, which meant that there were different chemical states or environments of phosphorus on the surface of the supports. Since P existed in the form of P<sup>5+</sup>, there were different coordination environments of P elements on the surface of Al<sub>2</sub>O<sub>3</sub>, namely phosphates with different forms, such as PO<sub>4</sub><sup>3-</sup>, HPO<sub>4</sub><sup>2-</sup> and H<sub>2</sub>PO<sub>4</sub><sup>-</sup> etc. For different types of phosphate compounds, the higher the degree of protonation of orthophosphate (i.e., PO<sub>4</sub><sup>3-</sup>), the higher its binding energy shifts. As shown in Table S5, the P 2P binding energy was measured. The binding energy of P 2p for PO<sub>4</sub><sup>3-</sup> was similar to that of 0.3Pθ-Al<sub>2</sub>O<sub>3</sub>, indicating that the P elements mainly exist in the form of PO<sub>4</sub><sup>3-</sup>. The P 2P binding energy of HPO<sub>4</sub><sup>2-</sup> is 133.4 eV [29], which is approximate to that of 0.6Pθ-Al<sub>2</sub>O<sub>3</sub>, indicating the HPO<sub>4</sub><sup>2-</sup> is the main form of phosphate on the surface of 0.6Pθ-Al<sub>2</sub>O<sub>3</sub>. The P 2p binding energy of H<sub>2</sub>PO<sub>4</sub><sup>-</sup> is 133.8 eV, similar to 1Pθ-Al<sub>2</sub>O<sub>3</sub>, 1.5Pθ-Al<sub>2</sub>O<sub>3</sub> and 3Pθ-Al<sub>2</sub>O<sub>3</sub>. It indicates that the H<sub>2</sub>PO<sub>4</sub><sup>-</sup>, which is connected with Al<sub>2</sub>O<sub>3</sub> by single bond, is the dominant phosphate compound on the surface of Al<sub>2</sub>O<sub>3</sub> when P content exceeds 1% [30].

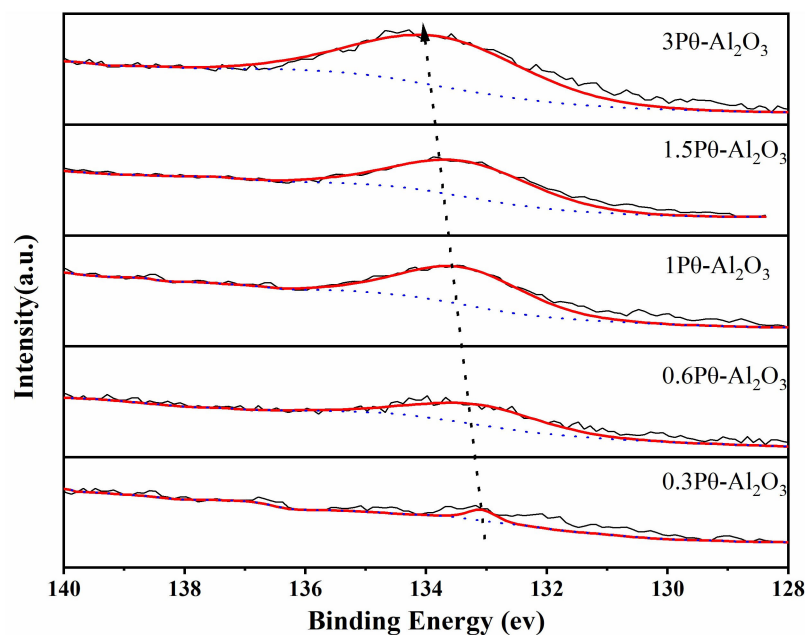


Figure 4. XPS spectra of P 2p for supports.

Therefore, combined with the results of IR and XPS, we believe that there are different forms of phosphate on the surface of the  $xP\theta\text{-Al}_2\text{O}_3$  supports prepared by the impregnation method, and the phosphate forms are related to the amount of P element. Figure 5 shows the relationship between phosphate configuration and phosphorus content on the surface of  $\theta\text{-Al}_2\text{O}_3$ . Specifically, when phosphorus is initially added to the support, phosphorus is most likely to form a multiple-bonds connection with the  $\text{Al}_2\text{O}_3$  support in the form of  $\text{PO}_4^{3-}$ , where one  $\text{PO}_4^{3-}$  replaces three hydroxyl groups on the surface of  $\text{Al}_2\text{O}_3$ . In this case, the function of phosphate is to replace the hydroxyl group on the surface of  $\theta\text{-Al}_2\text{O}_3$ , which reduces the hydroxyl content and leads to the increase of hydrophobicity. With the increase of P content, phosphates such as  $\text{HPO}_4^{2-}$  and  $\text{H}_2\text{PO}_4^-$  gradually dominate. It was worth noting that the dominant phosphate changed from  $\text{HPO}_4^{2-}$  to  $\text{H}_2\text{PO}_4^-$  when the content of P changed from 0.6 wt.% to 1 wt.%, which may account for the hydrophobicity of unmodified  $0P\theta\text{-Al}_2\text{O}_3$  ranging between  $0.6P\theta\text{-Al}_2\text{O}_3$  and  $1P\theta\text{-Al}_2\text{O}_3$ .

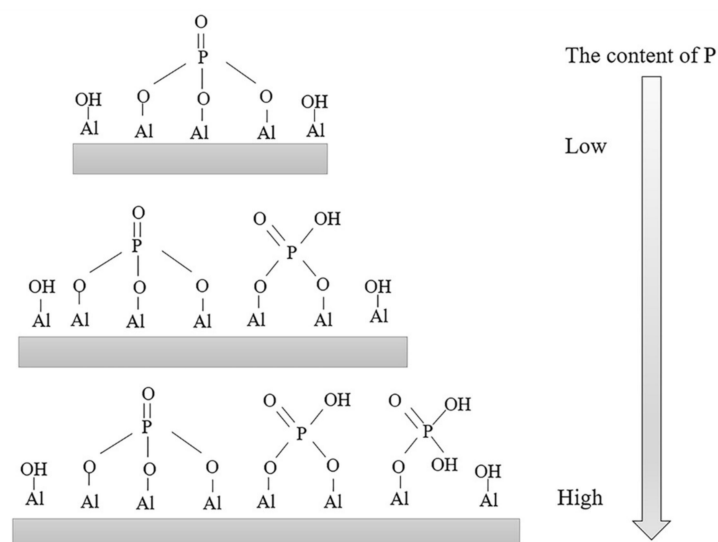


Figure 5. Profile of the relationship between phosphate compounds and phosphorus content on the surface of  $xP\theta\text{-Al}_2\text{O}_3$ .

## 2.2. Characterization of Catalysts

The XRD pattern of Pd/xP $\theta$ -Al<sub>2</sub>O<sub>3</sub> catalyst is shown in Figure 6. No obvious peaks of Pd or PdO are observed in all samples, indicating that Pd or PdO is well dispersed on the supports.

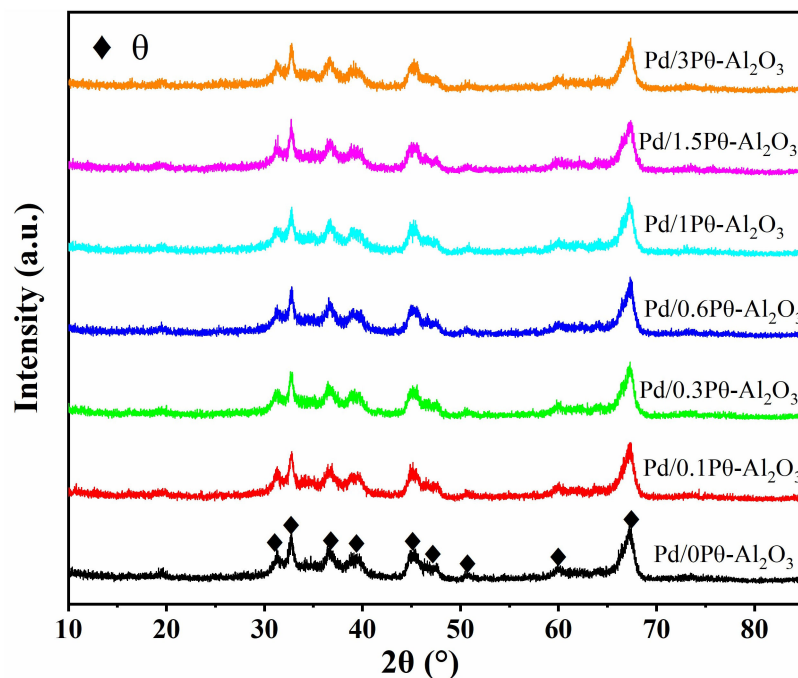
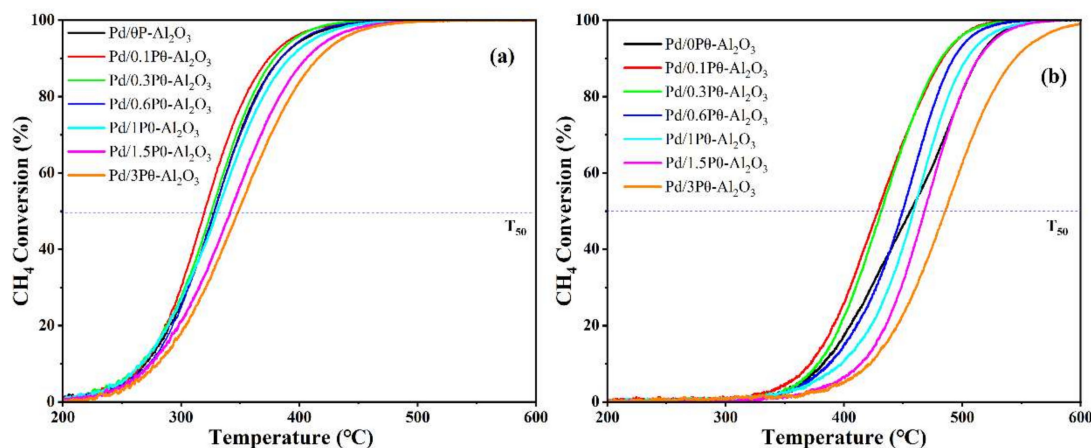


Figure 6. XRD patterns of Pd/xP $\theta$ -Al<sub>2</sub>O<sub>3</sub> samples.

In order to explore the influence of phosphorus loading on the activity of catalysts for methane catalytic combustion, the methane catalytic combustion activity of catalysts was tested. The light-off curves of lean-burn activity of catalysts in the absence and presence of water are shown in Figure 7. In the absence of water, Pd/0.1P $\theta$ -Al<sub>2</sub>O<sub>3</sub> catalyst had the lowest T<sub>50</sub> and the best catalytic activity for methane catalytic combustion among these catalysts. Compared with unmodified Pd/0P $\theta$ -Al<sub>2</sub>O<sub>3</sub> catalyst, Pd/xP $\theta$ -Al<sub>2</sub>O<sub>3</sub> (x = 0.1, 0.3, 0.6) shows better catalytic activity due to lower T<sub>50</sub> when the amount of modified element P is lower, however, excessive P content would decrease the activity of the catalyst. The activity of the catalyst in the absence of water decreased in the sequence: Pd/0.1P $\theta$ -Al<sub>2</sub>O<sub>3</sub> > Pd/0.3P $\theta$ -Al<sub>2</sub>O<sub>3</sub> > Pd/0.6P $\theta$ -Al<sub>2</sub>O<sub>3</sub> > Pd/0P $\theta$ -Al<sub>2</sub>O<sub>3</sub> > Pd/1P $\theta$ -Al<sub>2</sub>O<sub>3</sub> > Pd/1.5P $\theta$ -Al<sub>2</sub>O<sub>3</sub> > Pd/3P $\theta$ -Al<sub>2</sub>O<sub>3</sub>. In order to investigate the water inhibition resistance of the catalyst for methane catalytic combustion, 8% water was introduced into the reaction atmosphere. The main reason for choosing 8% water was that we had investigated the influence of different amounts of water on methane catalytic combustion (Figure S4). For Pd/Al<sub>2</sub>O<sub>3</sub> catalyst, the methane catalytic combustion activity decreased with the increase of the concentration of water in the reaction atmosphere, but the degree of decrease was small when the water concentration exceeded 8%, which was consistent with the results in the literature [31]. Therefore, 8% water was chosen. As shown in Figure 7b, the T<sub>50</sub> of all samples shifted to high temperatures of more than 100 °C when 8% water was added to the reaction atmosphere, and the activity sequence of samples in the presence of 8% water was consistent with samples in the absence of water condition, indicating that the addition of 8% water significantly inhibited the activity of the catalyst. Table 1 shows the T<sub>50</sub> results of the light-off test in the absence and presence of 8% water and the  $\Delta T_{50}$  results were calculated. Pd/0.1P $\theta$ -Al<sub>2</sub>O<sub>3</sub> showed the lowest T<sub>50</sub> and  $\Delta T_{50}$ , indicating that it had the best methane catalytic combustion activity and the best resistance to water inhibition. Studies have shown that the accumulation of hydroxyl groups on the Al<sub>2</sub>O<sub>3</sub> surface is the main reason for the water inhibition of Pd-based methane catalytic combustion catalysts [32]. Therefore, improving the hydrophobicity of the carrier or using a highly

hydrophobic carrier, such as SSZ-13 and Beta zeolite [12,33], is the key to solving the water inhibition problem. Combined with the above data on hydrophobicity, it was found that the variation rule of methane activity of the samples was consistent with the variation rule of the hydrophobicity of the carrier. Therefore, the addition of P element regulated the hydrophobicity of the support by changing the hydroxyl groups on the surface of  $\text{Al}_2\text{O}_3$ , thus affecting its methane catalytic combustion activity.



**Figure 7.** Light off test curves of Pd/xPθ- $\text{Al}_2\text{O}_3$  catalysts for methane catalytic combustion in the absence (a) and presence of 8% water. (b) Condition: 2000 ppmCH<sub>4</sub> + 5%O<sub>2</sub> + 0% $\text{H}_2\text{O}$  (or 8% $\text{H}_2\text{O}$ ) + N<sub>2</sub> balance, GHSV = 36,000 h<sup>-1</sup>.

**Table 1.** The T<sub>50</sub> of light-off test.

Samples	T <sub>50</sub> /°C		ΔT <sub>50</sub> /°C
	0% $\text{H}_2\text{O}$	8% $\text{H}_2\text{O}$	
Pd/θ $\text{Al}_2\text{O}_3$	328	455	127
Pd/0.1Pθ- $\text{Al}_2\text{O}_3$	320	428	108
Pd/0.3Pθ- $\text{Al}_2\text{O}_3$	326	431	105
Pd/0.6Pθ- $\text{Al}_2\text{O}_3$	328	449	121
Pd/1Pθ- $\text{Al}_2\text{O}_3$	330	458	128
Pd/1.5Pθ- $\text{Al}_2\text{O}_3$	341	468	127
Pd/3Pθ- $\text{Al}_2\text{O}_3$	349	485	136

(T<sub>50</sub>: the temperature at which methane conversion reaches 50%. ΔT<sub>50</sub> = T<sub>50wet</sub> – T<sub>50dry</sub>).

A TGA test was conducted to investigate the hydrophobic performance of catalysts loaded with Pd and the results are shown in Figure 8. The amount of water desorption can be calculated by the weight loss curve of the sample, which is shown in Table S7. The TGA test method was the same as that of the supports, so the amount of water desorption can reflect the hydrophobicity of the catalysts. Based on the results of water desorption of samples with different P content, it was found that the hydrophobicity of the catalysts decreased in the following sequence: Pd/0.1Pθ- $\text{Al}_2\text{O}_3$  > Pd/0.3Pθ- $\text{Al}_2\text{O}_3$  > Pd/0.6Pθ- $\text{Al}_2\text{O}_3$  > Pd/θ- $\text{Al}_2\text{O}_3$  > Pd/1Pθ- $\text{Al}_2\text{O}_3$  > Pd/1.5Pθ- $\text{Al}_2\text{O}_3$  > Pd/3Pθ- $\text{Al}_2\text{O}_3$ . This was consistent with the results of the hydrophobicity of the supports, indicating that the load of Pd does not change the hydrophobicity of the supports.

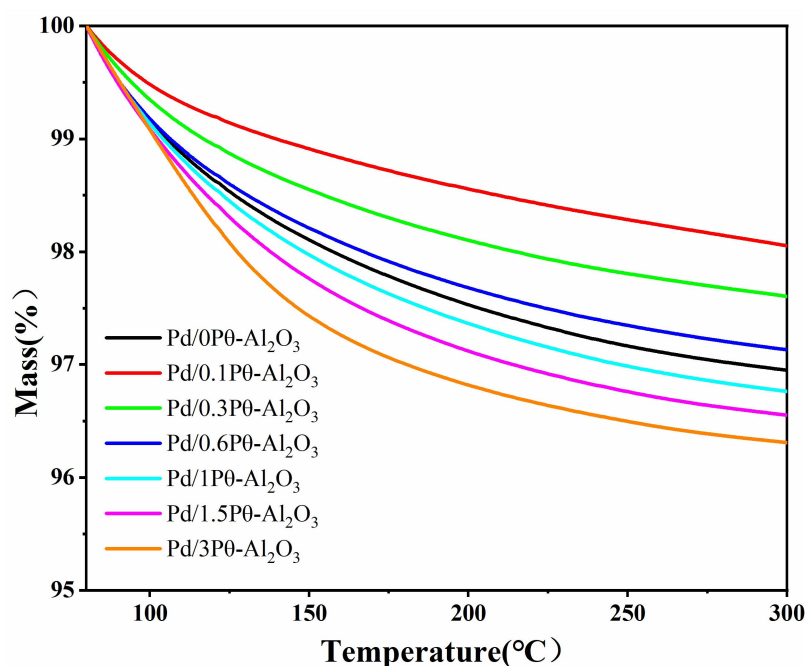


Figure 8. The weight loss curve of catalysts measured by TGA.

The hydrophobicity of the Al<sub>2</sub>O<sub>3</sub> is determined by the hydroxyl content on its surface, so the NH<sub>3</sub>-TPD test, which measured the hydroxyl content of the samples, can further confirm the changes of hydrophobicity in the samples. Results are shown in Figure 9. The desorption curves of NH<sub>3</sub> of the samples had two peaks, which were similar to those of supports. Therefore, the peak 1 was attributed to the B acid produced by the hydroxyl groups on the surface of θ-Al<sub>2</sub>O<sub>3</sub>. The integral results of the curve of peak 1 is shown in Table S8. The law between the relative surface hydroxyl density and phosphorus content of the samples was consistent with that of hydrophobicity mentioned above, which once again proves that phosphates replaced the hydroxyl groups of θ-Al<sub>2</sub>O<sub>3</sub> to regulate hydrophobicity.

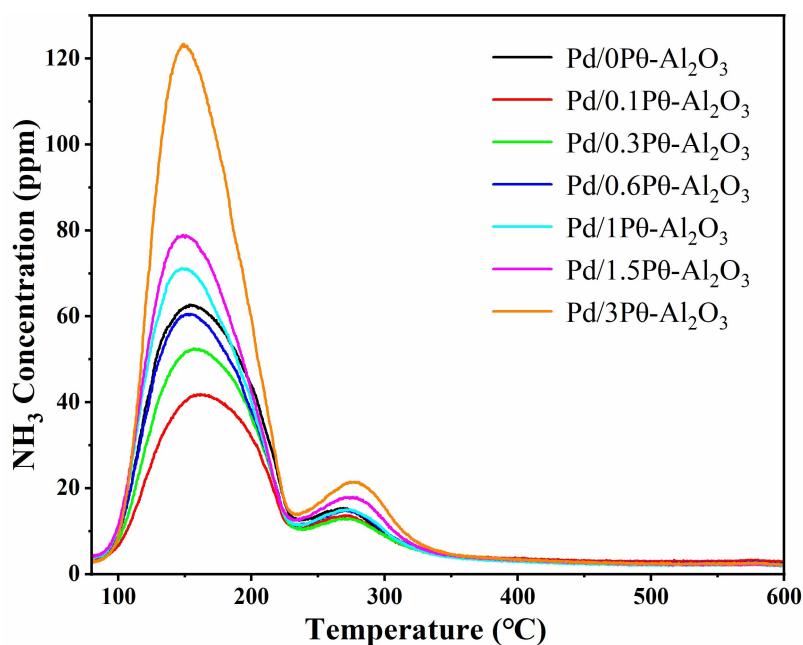
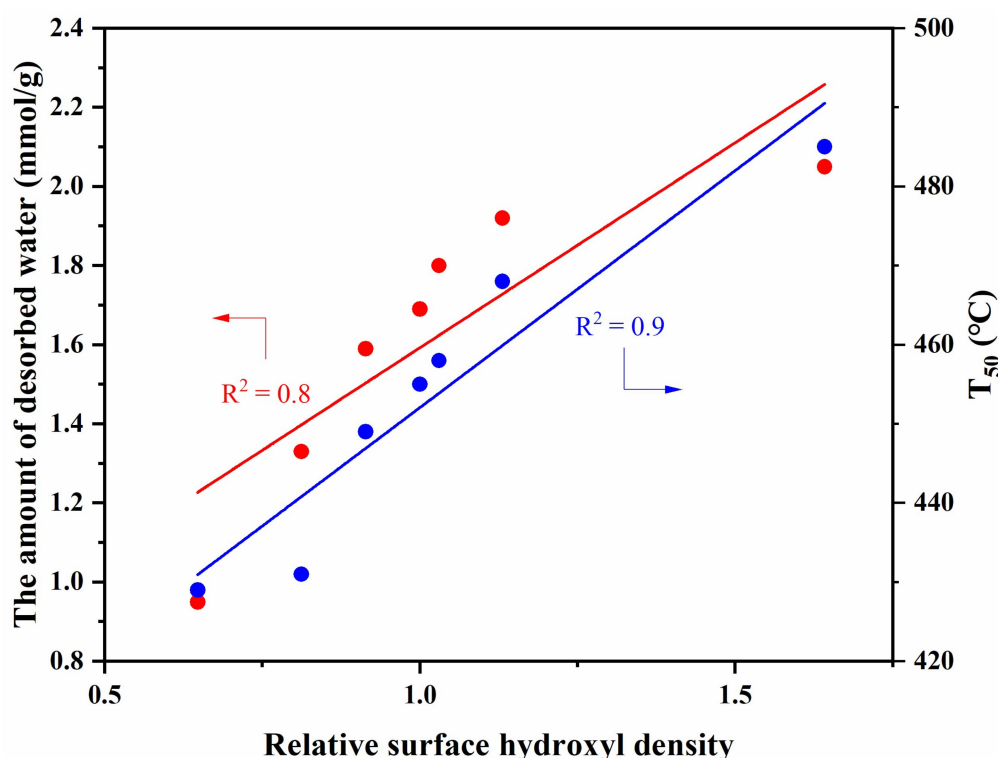


Figure 9. NH<sub>3</sub>-TPD profiles of the catalysts.

The relationship between the catalytic methane oxidation activity of the samples and the hydrophobicity of the supports has been discussed above. In order to illustrate that the addition of P would not change the active site, which is PdO species [34,35], the kinetic experiment of the sample under the condition that methane oxidation conversion rate was less than 20% in the presence of 8% water was tested. As shown in Figure S5 and Table S9, the activation energy of the samples was the same, which indicated that the active center of the samples did not change after the addition of phosphorus. In addition, the results of activation energy were in well line with the results of catalytic activity. On this basis, the relative surface hydroxyl density of supports was correlated with the hydrophobicity of supports and the  $T_{50}$  of the methane catalytic combustion ignition test (Figure 10), showing an approximate linear relationship, which indicated that the activity, hydrophobicity, and surface hydroxyl density of the sample were interrelated.



**Figure 10.** Plot of relative surface hydroxyl density with hydrophobicity (the amount of desorbed water) and methane oxidation activity ( $T_{50}$  tested in the presence of 8% water).

### 3. Materials and Methods

#### 3.1. Catalysts Preparation

The  $\theta$ - $\text{Al}_2\text{O}_3$  was prepared by calcining commercial  $\gamma$ - $\text{Al}_2\text{O}_3$  at 1050 °C for 2 h in air. P-modified  $\theta$ - $\text{Al}_2\text{O}_3$  supports were prepared by incipient wetness impregnation method and  $(\text{NH}_4)_2\text{HPO}_4$  was employed as the material source for phosphorus. Specifically, prior to impregnation, the saturated water absorption of the carrier was tested.  $(\text{NH}_4)_2\text{HPO}_4$  was then dissolved into a certain amount of water to make the desired impregnation solution, which was then loaded on  $\theta$ - $\text{Al}_2\text{O}_3$ . The mixtures of impregnation solution and the support were slightly stirred so that the solution containing P was completely mixed with the  $\text{Al}_2\text{O}_3$  support to ensure an even load, then the  $\theta$ - $\text{Al}_2\text{O}_3$  supports impregnated with different amounts of phosphorus were placed at room temperature for 12 h, dried overnight at 80 °C, and finally calcined at 500 °C in air for 4 h. The phosphorus content of the supports were denoted as x wt.% (x = 0, 0.1, 0.3, 0.6, 1, 1.5, 3) and the supports were named as xP $\theta$ - $\text{Al}_2\text{O}_3$ .

The Pd-based catalysts were prepared by incipient wetness impregnation method, Taking the as-obtained P-doped  $\theta$ - $\text{Al}_2\text{O}_3$  as carriers using  $\text{Pd}(\text{NO}_3)_2$  aqueous solution as

the precursor. The as-prepared samples were placed at room temperature for 12 h, dried overnight at 80 °C, and calcined at 500 °C in air for 4 h. The nominal Pd loading was 0.8 wt.%. The samples were named as Pd/xP0-Al<sub>2</sub>O<sub>3</sub> (x = 0, 0.1, 0.3, 0.6, 1, 1.5, 3).

### 3.2. Characterization

X-ray powder diffraction was conducted on a Bruker D8 Focus equipped with Cu K $\alpha$ 1 radiation ( $\lambda = 1.54056 \text{ \AA}$ ). The test angle range was 5–85° with a step length of 0.01°. All patterns were collected at 40 kV and 30 mA.

The N<sub>2</sub> isotherms were measured using Micromeritics ASAP 2460 instrument (Micromeritics, Norcross, GA, USA). Before the test, the samples were degassed at 300 °C for 12 h under vacuum to remove water vapor adsorbed in the sample. The specific surface area and the mesoporous volume were calculated using the Brunauer–Emmett–Teller (BET) and Barrett–Joyner–Halenda models (BJH), respectively.

The amount of phosphorus and palladium element were determined by inductively coupled plasma-optical emission spectrometer (ICP-OES, Plasma 1500, NCS, Guangzhou, China).

TG was conducted on a Mettler-Toledo Thermal Analysis instrument. Prior to the experiment, the samples were treated in a constant temperature and humidity instrument for 12 h until the catalysts adsorbed water to a saturation condition under 80% humidity at 80 °C.

NH<sub>3</sub> temperature-programmed desorption (NH<sub>3</sub>-TPD) was conducted on home-made equipment. After oxidizing the samples for 30 min at 500 °C in a 5%O<sub>2</sub>/N<sub>2</sub> flow and cooling down to 80 °C in a N<sub>2</sub> flow, a mixed gas flow ([NH<sub>3</sub>] = 500 ppm, balanced with N<sub>2</sub>, flow rate = 500 mL·min<sup>-1</sup>) was switched over into the reactor and NH<sub>3</sub> adsorption was completed after 2 h at 80 °C. Then, at the constant temperature, physisorbed NH<sub>3</sub> was purged with a N<sub>2</sub> flow. Ramp the reactor to 600 °C at a heating rate of 10 °C min<sup>-1</sup> and the concentrations of desorbed NH<sub>3</sub> were recorded by a MKS 2030 gas cell Fourier-transform infrared spectroscopy.

IR spectroscopy was conducted on a Nicolet 6700 spectrometer. The time-resolved spectrum with a range of 400–4000 cm<sup>-1</sup> and a resolution of 4 cm<sup>-1</sup> was collected. The DRIFT spectrum of KBr was used as the background spectrum.

X-ray photoelectron spectroscopy (XPS) measurements were obtained by a K-Alpha (Thermo Fisher Scientific, Waltham, MA, USA) spectrometer. P 2p photoelectron spectra were collected for each sample. The electronic binding energy of reference C 1s was 284.8 eV.

### 3.3. Catalytic Activity Test

The methane catalytic combustion tests with and without water were performed in a home-made fixed-bed reactor. Specifically, the 0.1 g granulated samples (60–80 mesh) were weighed, mixing with 0.9 g quartz sand (60–80 mesh), and loaded into a quartz U-shaped reactor filled with quartz wool, which constitutes a fixed-bed reactor.

The process of the catalyst performance test was as follows: the samples were pre-treated first, and the specific operation was as follows: the reaction gas (2000 ppm CH<sub>4</sub>, 5%O<sub>2</sub>, 8%H<sub>2</sub>O (0%H<sub>2</sub>O), N<sub>2</sub> was the equilibrium gas, and the space velocity was 36,000 h<sup>-1</sup>) was fed into the reactor and the reactor was heated to 600 °C, at which temperature the catalytic oxidation of methane can be completely converted in the presence or absence of water, then the reaction gas and the temperature was maintained for 1 h so that the samples reached a stable state. Next, the ignition test of methane catalytic combustion of the sample could be carried out. First, the sample was cooled at 80 °C, and then the reaction gas was injected into the reactor and stabilized, and the ignition test of methane complete oxidation was then conducted. The concentration of the gas was detected by Fourier infrared gas analyzer (MKS). The methane conversion was calculated as the following:

$$\text{Methane conversion} = \frac{[\text{CH}_4]_{\text{in}} - [\text{CH}_4]_{\text{out}}}{[\text{CH}_4]_{\text{in}}} \times 100\%$$

The kinetic experiments were conducted on the same experimental equipment as the activity tests. Prior to testing, the samples were granulated (60–80 mesh) to exclude external diffusion. The method to eliminate the external diffusion was to increase the space velocity at a constant kinetic temperature until the reaction rate would not change. On this basis, the kinetic experiments of methane oxidation were tested under the condition that the methane conversion rate was less than 20%.

#### 4. Conclusions

In conclusion, P-modified  $\theta$ - $\text{Al}_2\text{O}_3$  supports were prepared by incipient wetness impregnation method. The phosphorus replaced the hydroxyl groups on the surface of  $\theta$ - $\text{Al}_2\text{O}_3$  in the form of phosphates ( $\text{PO}_4^{3-}$ ,  $\text{HPO}_4^{2-}$ ,  $\text{H}_2\text{PO}_4^-$ ), thus regulating the hydrophobicity of the  $\theta$ - $\text{Al}_2\text{O}_3$ . When a small amount of P element was added, the as-prepared  $x\text{P-}\theta\text{Al}_2\text{O}_3$  ( $x = 0.1, 0.3, 0.6$ ) supports had better hydrophobicity than the unmodified  $\theta$ - $\text{Al}_2\text{O}_3$  support, and had better resistance to water inhibition when used as the support for methane catalytic combustion. Overall, doping a small amount of phosphorus element can improve the methane catalytic combustion performance and the ability of resistance to water inhibition of  $\text{Pd}/\theta\text{-Al}_2\text{O}_3$  catalyst, which provides a feasible idea to solve the problem of methane catalytic combustion water inhibition.

**Supplementary Materials:** The following supporting information can be downloaded at: <https://www.mdpi.com/article/10.3390/catal13040709/s1>, Table S1: The content of phosphorus of P modified supports, Table S2: The specific surface area and pore volume of the supports, Table S3: Quantitative results of TG test of supports, Table S4: Quantitative results of  $\text{NH}_3$ -TPD test of supports, Table S5: Binding energy of P 2p, Table S6: Element content of Pd catalysts, Table S7: Quantitative results of TG test of samples, Table S8: Quantitative results of  $\text{NH}_3$ -TPD test of samples, Table S9: Apparent activation energy of samples in the presence 8% water. Figure S1: XRD patterns of the commercial  $\gamma$ - $\text{Al}_2\text{O}_3$  calcined at different temperature; Figure S2: XRD patterns of the  $x\text{P}\theta\text{-Al}_2\text{O}_3$  supports, Figure S3: FT-IR profiles of supports, Figure S4: Catalytic combustion of methane over  $\text{Pd}/\gamma\text{-Al}_2\text{O}_3$  with different amounts of water, Figure S5: The Arrhenius curves of the samples in the presence of 8% water.

**Author Contributions:** Conceptualization, W.X., J.W. (Jun Wang), C.W. and M.S.; Methodology, W.X., J.W. (Jianqiang Wang) and G.S.; Validation, W.X. and Y.W.; Formal analysis, W.X., J.W. (Jun Wang) and Y.W.; Investigation, W.X. and Y.W.; Resources, J.W. (Jun Wang) and M.S.; Writing—Original Draft, W.X. and Y.W.; Writing—Review & Editing, J.W. (Jun Wang), J.W. (Jianqiang Wang), G.S. and M.S.; Funding Acquisition, J.W. (Jun Wang) and M.S. All authors have read and agreed to the published version of the manuscript.

**Funding:** This work was supported by the Key R&D project of Shandong Province (2021CXGC010703, 2022CXGC020311) and National Key R&D Program of China (2021YFB3503200).

**Data Availability Statement:** The research data can be acquired from the corresponding author upon reasonable request.

**Acknowledgments:** The authors are grateful for the supports given by Innovative Research Groups of the National Natural Science Foundation of China (51921004) and National Rare Earth Catalysis Research Institute.

**Conflicts of Interest:** The authors declare no conflict of interest.

#### References

1. Liu, H.; Zhao, B.; Chen, Y.; Ren, C.; Chen, Y. Rare earths (Ce, Y, Pr) modified  $\text{Pd}/\text{La}_2\text{O}_3\text{ZrO}_2\text{Al}_2\text{O}_3$  catalysts used in lean-burn natural gas fueled vehicles. *J. Rare Earths* **2017**, *35*, 1077–1082. [[CrossRef](#)]
2. Auvray, X.; Lindholm, A.; Milh, M.; Olsson, L. The addition of alkali and alkaline earth metals to  $\text{Pd}/\text{Al}_2\text{O}_3$  to promote methane combustion. Effect of Pd and Ca loading. *Catal. Today* **2018**, *299*, 212–218. [[CrossRef](#)]
3. Mirkelamoglu, B.; Ozkan, U.S. Effect of water vapor on the activity and stability of  $\text{Pd}/\text{SZ}$  and  $\text{Co}/\text{ZrO}_2$  in dual-catalyst treatment of simulated exhaust from lean-burn natural gas engines. *Appl. Catal. B Environ.* **2010**, *96*, 421–433. [[CrossRef](#)]
4. Hutter, R.; De Libero, L.; Elbert, P.; Onder, C.H. Catalytic methane oxidation in the exhaust gas aftertreatment of a lean-burn natural gas engine. *Chem. Eng. J.* **2018**, *349*, 156–167. [[CrossRef](#)]

5. Hong, E.; Kim, C.; Lim, D.-H.; Cho, H.-J.; Shin, C.-H. Catalytic methane combustion over Pd/ZrO<sub>2</sub> catalysts: Effects of crystalline structure and textural properties. *Appl. Catal. B Environ.* **2018**, *232*, 544–552. [[CrossRef](#)]
6. Mowery, D.L.; Graboski, M.S.; Ohno, T.R.; McCormick, R.L. Deactivation of PdO-Al<sub>2</sub>O<sub>3</sub> oxidation catalyst in lean-burn natural gas engine exhaust: Aged catalyst characterization and studies of poisoning by H<sub>2</sub>O and SO<sub>2</sub>. *Appl. Catal. B Environ.* **1999**, *21*, 157–169. [[CrossRef](#)]
7. Fan, C.; Yang, L.; Luo, L.; Wu, Z.W.; Qin, Z.F.; Zhu, H.Q.; Fan, W.B.; Wang, J.G. A highly active Pd/H-ZSM-5 catalyst in lean methane combustion prepared via a sol-gel method and treated by reduction-oxidation. *New J. Chem.* **2020**, *44*, 3940–3949. [[CrossRef](#)]
8. Huang, W.; Zhang, X.; Yang, A.-C.; Goodman, E.D.; Kao, K.-C.; Cargnello, M. Enhanced Catalytic Activity for Methane Combustion through in Situ Water Sorption. *ACS Catal.* **2020**, *10*, 8157–8167. [[CrossRef](#)]
9. Gholami, R.; Alyani, M.; Smith, K. Deactivation of Pd Catalysts by Water during Low Temperature Methane Oxidation Relevant to Natural Gas Vehicle Converters. *Catalysts* **2015**, *5*, 561–594. [[CrossRef](#)]
10. Gao, D.; Wang, S.; Zhang, C.; Yuan, Z.; Wang, S. Methane Combustion over Pd/Al<sub>2</sub>O<sub>3</sub> Catalyst: Effects of Chlorine Ions and Water on Catalytic Activity. *Chin. J. Catal.* **2008**, *29*, 1221–1225. [[CrossRef](#)]
11. Ciuparu, D.; Perkins, E.; Pfefferle, L. In situ DR-FTIR investigation of surface hydroxyls on gamma-Al<sub>2</sub>O<sub>3</sub> supported PdO catalysts during methane combustion. *Appl. Catal. A Gen.* **2004**, *263*, 145–153. [[CrossRef](#)]
12. Losch, P.; Huang, W.; Vozniuk, O.; Goodman, E.D.; Schmidt, W.; Cargnello, M. Modular Pd/Zeolite Composites Demonstrating the Key Role of Support Hydrophobic/Hydrophilic Character in Methane Catalytic Combustion. *ACS Catal.* **2019**, *9*, 4742–4753. [[CrossRef](#)]
13. Cui, Y.; Chen, J.Z.; Peng, B.; Kovarik, L.; Devaraj, A.; Li, Z.; Ma, T.; Wang, Y.; Szanyi, J.; Miller, J.T.; et al. Onset of High Methane Combustion Rates over Supported Palladium Catalysts: From Isolated Pd Cations to PdO Nanoparticles. *JACS Au* **2021**, *1*, 396–408. [[CrossRef](#)]
14. Chen, X.; Lin, J.; Zheng, Y.; Zhan, Y.; Zhang, W.; Xiao, Y.; Zheng, Y.; Jiang, L. Catalytic methane oxidation performance over Pd/γ-Al<sub>2</sub>O<sub>3</sub> catalyst optimized by the synergy of phosphorus and MO<sub>x</sub> (M = La, Ba and Zr). *Fuel* **2021**, *299*, 120933. [[CrossRef](#)]
15. Friberg, I.; Sadokhina, N.; Olsson, L. Complete methane oxidation over Ba modified Pd/Al<sub>2</sub>O<sub>3</sub>: The effect of water vapor. *Appl. Catal. B Environ.* **2018**, *231*, 242–250. [[CrossRef](#)]
16. Zou, X.; Rui, Z.; Song, S.; Ji, H. Enhanced methane combustion performance over NiAl<sub>2</sub>O<sub>4</sub>-interface-promoted Pd/γ-Al<sub>2</sub>O<sub>3</sub>. *J. Catal.* **2016**, *338*, 192–201. [[CrossRef](#)]
17. Shen, J.; Hayes, R.E.; Wu, X.; Semagina, N. 100° Temperature Reduction of Wet Methane Combustion: Highly Active Pd–Ni/Al<sub>2</sub>O<sub>3</sub> Catalyst versus Pd/NiAl<sub>2</sub>O<sub>4</sub>. *ACS Catal.* **2015**, *5*, 2916–2920. [[CrossRef](#)]
18. Wang, J.; Wang, Y.; Wen, J.; Shen, M.; Wang, W. Effect of phosphorus introduction strategy on the surface texture and structure of modified alumina. *Microporous Mesoporous Mater.* **2009**, *121*, 208–218. [[CrossRef](#)]
19. Li, A.; Wang, Y.-H.; Ren, J.; Zhang, J.-L.; Li, W.; Guo, C.-L. Enhanced catalytic activity and stability over P-modified alumina supported Pd for anthraquinone hydrogenation. *Appl. Catal. A Gen.* **2020**, *593*, 117422. [[CrossRef](#)]
20. Murata, K.; Ohyama, J.; Yamamoto, Y.; Arai, S.; Satsuma, A. Methane Combustion over Pd/Al<sub>2</sub>O<sub>3</sub> Catalysts in the Presence of Water: Effects of Pd Particle Size and Alumina Crystalline Phase. *ACS Catal.* **2020**, *10*, 8149–8156. [[CrossRef](#)]
21. Wang, J.; Bokhimi, X.; Morales, A.; Novaro, O.; Lopez, T.; Gomez, R. Aluminum local environment and defects in the crystalline structure of Sol–Gel alumina catalyst. *J. Phys. Chem. B* **1999**, *103*, 299–303. [[CrossRef](#)]
22. Chen, X.; Zheng, Y.; Huang, F.; Xiao, Y.; Cai, G.; Zhang, Y.; Zheng, Y.; Jiang, L. Catalytic Activity and Stability over Nanorod-Like Ordered Mesoporous Phosphorus-Doped Alumina Supported Palladium Catalysts for Methane Combustion. *ACS Catal.* **2018**, *8*, 11016–11028. [[CrossRef](#)]
23. Keshavarz, A.R.; Rezaei, M.; Yaripour, F. Preparation of nanocrystalline γ-Al<sub>2</sub>O<sub>3</sub> catalyst using different procedures for methanol dehydration to dimethyl ether. *J. Nat. Gas Chem.* **2011**, *20*, 334–338. [[CrossRef](#)]
24. Wang, D.; Jangjou, Y.; Liu, Y.; Sharma, M.K.; Luo, J.; Li, J.; Kamasamudram, K.; Epling, W.S. A comparison of hydrothermal aging effects on NH<sub>3</sub>-SCR of NO<sub>x</sub> over Cu-SSZ-13 and Cu-SAPO-34 catalysts. *Appl. Catal. B Environ.* **2015**, *165*, 438–445. [[CrossRef](#)]
25. Klimov, O.; Nadeina, K.; Vatutina, Y.V.; Stolyarova, E.; Danilova, I.; Gerasimov, E.Y.; Prosvirin, I.; Noskov, A. CoMo/Al<sub>2</sub>O<sub>3</sub> hydrotreating catalysts of diesel fuel with improved hydrodenitrogenation activity. *Catal. Today* **2018**, *307*, 73–83. [[CrossRef](#)]
26. Persson, P.; Nilsson, N.; Sjöberg, S. Structure and bonding of orthophosphate ions at the iron oxide–aqueous interface. *J. Colloid Interface Sci.* **1996**, *177*, 263–275. [[CrossRef](#)] [[PubMed](#)]
27. Dong, J.; Wang, J.; Wang, J.; Yang, M.; Li, W.; Shen, M. Enhanced thermal stability of palladium oxidation catalysts using phosphate-modified alumina supports. *Catal. Sci. Technol.* **2017**, *7*, 5038–5048. [[CrossRef](#)]
28. Sigurdson, S.; Sundaramurthy, V.; Dalai, A.; Adjaye, J. Phosphorus promoted trimetallic NiMoW/γ-Al<sub>2</sub>O<sub>3</sub> sulfide catalysts in gas oil hydrotreating. *J. Mol. Catal. A Chem.* **2008**, *291*, 30–37. [[CrossRef](#)]
29. Puziy, A.; Poddubnaya, O.; Ziatdinov, A. On the chemical structure of phosphorus compounds in phosphoric acid-activated carbon. *Appl. Surf. Sci.* **2006**, *252*, 8036–8038. [[CrossRef](#)]
30. Fitz, C.W., Jr.; Rase, H.F. Effects of phosphorus on nickel-molybdenum hydrodesulfurization/hydrodenitrogenation catalysts of varying metals content. *Ind. Eng. Chem. Prod. Res. Dev.* **1983**, *22*, 40–44. [[CrossRef](#)]
31. Kikuchi, R.; Maeda, S.; Sasaki, K.; Wennerström, S.; Eguchi, K. Low-temperature methane oxidation over oxide-supported Pd catalysts: Inhibitory effect of water vapor. *Appl. Catal. A Gen.* **2002**, *232*, 23–28. [[CrossRef](#)]

32. Persson, K.; Pfefferle, L.D.; Schwartz, W.; Ersson, A.; Järås, S.G. Stability of palladium-based catalysts during catalytic combustion of methane: The influence of water. *Appl. Catal. B Environ.* **2007**, *74*, 242–250. [[CrossRef](#)]
33. Friberg, I.; Sadokhina, N.; Olsson, L. The effect of Si/Al ratio of zeolite supported Pd for complete CH<sub>4</sub> oxidation in the presence of water vapor and SO<sub>2</sub>. *Appl. Catal. B Environ.* **2019**, *250*, 117–131. [[CrossRef](#)]
34. Bunting, R.J.; Cheng, X.; Thompson, J.; Hu, P. Amorphous Surface PdOX and Its Activity toward Methane Combustion. *ACS Catal.* **2019**, *9*, 10317–10323. [[CrossRef](#)]
35. Stotz, H.; Maier, L.; Boubnov, A.; Gremminger, A.T.; Grunwaldt, J.D.; Deutschmann, O. Surface reaction kinetics of methane oxidation over PdO. *J. Catal.* **2019**, *370*, 152–175. [[CrossRef](#)]

**Disclaimer/Publisher's Note:** The statements, opinions and data contained in all publications are solely those of the individual author(s) and contributor(s) and not of MDPI and/or the editor(s). MDPI and/or the editor(s) disclaim responsibility for any injury to people or property resulting from any ideas, methods, instructions or products referred to in the content.